Classification:

Biological Sciences – Neuroscience

Title:

Satiety, Thermosensation and Mechanosensation Regulate a Spontaneous *C. elegans* Sleep State

Authors:

Daniel L. Gonzales[1,2], Jasmine Zhou[3], Jacob T. Robinson[1-4*]

Affiliations:

[1] Applied Physics Program, Rice University, 6100 Main St., Houston, TX 77005, USA.

[2] Department of Electrical and Computer Engineering, Rice University, 6100 Main St., Houston, TX 77005, USA.

[3] Department of Bioengineering, Rice University, 6100 Main St., Houston, TX 77005, USA.

[4] Department of Neuroscience, Baylor College of Medicine, One Baylor Plaza, Houston, TX 77030, USA.

*Correspondence to: jtrobinson@rice.edu.

Abstract:

One remarkable feature of the nervous system is its ability to rapidly and spontaneously switch between activity states. In the extreme example of sleep, animals arrest locomotion, reduce their sensitivity to sensory stimuli, and dramatically alter their neural activity. Small organisms are useful models to better understand these sudden changes in neural states because we can simultaneously observe whole-brain activity, monitor behavior and precisely regulate the external environment. Here, we show a spontaneous sleep-like behavior in *C. elegans* that is associated with a distinct global-brain state and regulated by both the animal's internal physiological state and input from multiple sensory circuits. Specifically, we found that when confined in microfluidic chambers, adult worms spontaneously transition between periods of normal activity and short quiescent bouts, with behavioral state transitions occurring every few minutes. This quiescent state, which we call μSleep, meets the behavioral requirements of *C. elegans* sleep, is dependent on known sleep-promoting neurons ALA and RIS, and is associated with a global down-regulation of neural activity. Consistent with prior studies of *C. elegans* sleep, we found that μSleep is regulated by satiety and temperature. In addition, we show for the first time that quiescence can be either driven or suppressed by thermosensory input, and that animal restraint induces quiescence through mechanosensory pathways. Together, these results establish a rich model system for studying how neural and behavioral state transitions are influenced by multiple physiological and environmental conditions.

Keywords:

C. elegans, sleep, multisensory integration, whole-brain imaging

Significance Statement:

Unique brain states govern animal behaviors like sleep and wakefulness; however, how the brain regulates these dramatic state transitions is not well understood. Brain activity can be influenced by a complex interaction between sensory circuits that monitor the external environment, neural circuits that control behavior, and internal chemical signaling. Here, we describe a platform to study behavioral states in a context that allows us to record whole-brain activity while controlling the environment and monitoring animal behavior. Specifically, we identify a pattern of sleep bouts in the roundworm *C. elegans* that occur when they are confined to microscopic fluidic chambers. This behavior platform provides a powerful system to study how neural circuits interact with chemical signaling to drive brain state transitions.

Introduction:

Understanding how animals select behaviors based on sensory information is a fundamental goal of neuroscience (1–4); however, sensorimotor transformations can vary dramatically depending on the state of the animal's nervous system (5–8). Wakefulness and arousal (9, 10), locomotor activity states (11, 12), satiety (13), attention (14), and emotions (5, 6, 15) represent a spectrum of physiological and neural states that can dramatically affect how animals respond to a given stimuli. Small animals like the nematode *C. elegans* are tractable model organisms for understanding how physiological and neural states combine with information from multiple sensory pathways and give rise to specific behavior (3, 6, 8, 13, 16–21).

Sleep is one example of a neural state that dramatically alters an animal's sensorimotor transformations (22, 23). Studies of sleep across the phylogenetic tree have shown that sensory systems transition to a reduced activity state that leads to a decreased animal response to external stimuli (24–28). Additionally, sleep and wakefulness have been shown to correspond with distinct patterns of neural activity in humans (22, 23), cats (29), rodents (23), and fruit flies (30, 31). Likewise, whole-brain recordings from *C. elegans* suggest that the majority of worm brain activity can be represented on a low-dimensional manifold (32), and that the activity on this manifold shifts from phasic to fixed-point attractor dynamics during developmental sleep (33). Additionally, studies with *C. elegans* have revealed molecular pathways (25, 34–37), neural circuits (34, 38–43), and neuropeptides (39, 42, 44, 45) that drive nematode sleep and arousal, and some of these mechanisms are conserved in in other animals (46–48). These reports have paved the way for using *C. elegans* sleep as a model system to understand spontaneous brain-state transitions between sleep and wakefulness. Given the number of unique regulators of *C.*

elegans sleep, there is a need to identify a behavior that facilitates our understanding of how brain-wide neural circuits transduce multiple external and internal factors to drive sleep-wake transitions. Here, we describe a *C. elegans* sleep behavior in a microfluidic environment, termed "μSleep," that is amenable to whole-brain imaging and is regulated both by the animal's physiological state and external sensory queues. While μSleep is likely a form of previously-reported nematode quiescence behaviors, such as stress-induced sleep and episodic swimming (40, 49), the rapid rate of state transitions and the fact that these quiescence behaviors occur in microfluidic devices provides and number of advantages for studying the mechanisms of state transitions with precise environmental controllability, high-throughput screenings and whole-brain imaging.

Results:

When confined to microfluidic chambers we found that adult *C. elegans* rapidly and spontaneously switch between normal activity and brief quiescent bouts without any additional stimuli (Fig. 1A). We initially observed this behavior when immobilizing worms for recording body-wall muscle electrophysiology (50). In these electrical recordings we observed minutes-long periods of muscle inactivity that corresponded to whole-animal quiescence (50). We have since found that this quiescence occurs in a wide range of microfluidic geometries (Movie S1-S2).

We found that the onset, frequency, and duration of quiescent bouts in microfluidic chambers are unique compared to previously-reported sleep behaviors in adult *C. elegans*. While larval *C. elegans* display quiescence during lethargus (25), quiescence in adult worms occurs in only a few situations, such as after several hours of swimming (49, 51–53) or after exposure to extreme environmental conditions (40, 44, 45, 54, 55). To determine how microfluidic-induced

quiescence compares to the well-established "episodic behavior" that occurs in swimming animals and "stress-induced quiescence" that occurs from a 30 min heat shock, we quantified these behaviors using the same methods to analyze μSleep (Fig. 1B-F). During a 4 hr imaging period, we found that animals partially immobilized in microfluidic channels (50 μm width, ~0.004 μL per chamber, Movie S2) displayed short (1.3 ± 0.1 min, mean ± sem, Fig. 1E) bouts that, on average, began within the first hour of imaging (51 ± 4 min, mean ± sem, Fig. 1D). Likewise, we also observed frequent, but longer (2.4 ± 0.3 min, mean ± sem, Fig. 1E) quiescent bouts when the microfluidic chambers were large enough to allow animals to swim (500 μm width, ~0.1 μL per chamber, Movie S1). We compared these data to swimming-induced quiescence, where animals alternate between swimming and quiescence in a large multi-well device or "WorMotel" (Fig. 1B, 8 μL of buffer per well) (56). In WorMotel, we recorded 5-7 times less sleep over the imaging period compared to microfluidic chambers (Fig. 1C) and longer quiescent bouts compared to either microfluidic geometry (3.6 ± 0.3 min, mean ± sem, Fig. 1E). Additionally, the average quiescence onset time was more than double what we observed for μSleep (175 ± 6 min, mean ± sem, Fig. 1D). For our final comparison point, we heat-shocked animals in the large microfluidic device for 30 min at 30 °C to record stress-induced quiescence (40) (Fig. 1B). As expected, during the noxious heat stimulus animals displayed their first quiescent bout more than 4-6 times faster than in microfluidic chambers with no external heat applied (13 ± 0.7 min, mean ± sem, Fig. 1D).

These initial data show that compared to episodic swimming in WorMotel, μSleep occurs with a higher frequency, faster onset and in shorter bouts (Fig. 1C-E). Similarly, μSleep onset occurs on a significantly different timescale compared to stress-induced sleep (Fig. 1B, D). It is important to note that while the μSleep phenotype shows a number of quantitative differences

when compared to episodic swimming and stress-induced quiescence, it is not clear if microfluidic-induced quiescence can be classified as a new *C. elegans* behavior. It is possible that the microfluidic environment accelerates episodic swimming or introduces mild stressors that more slowly lead to stress-induced quiescence. Thus, we consider μSleep behavior to be phenotypically distinct from other reported quiescent behaviors in *C. elegans* adults, and not necessarily a new behavioral state.

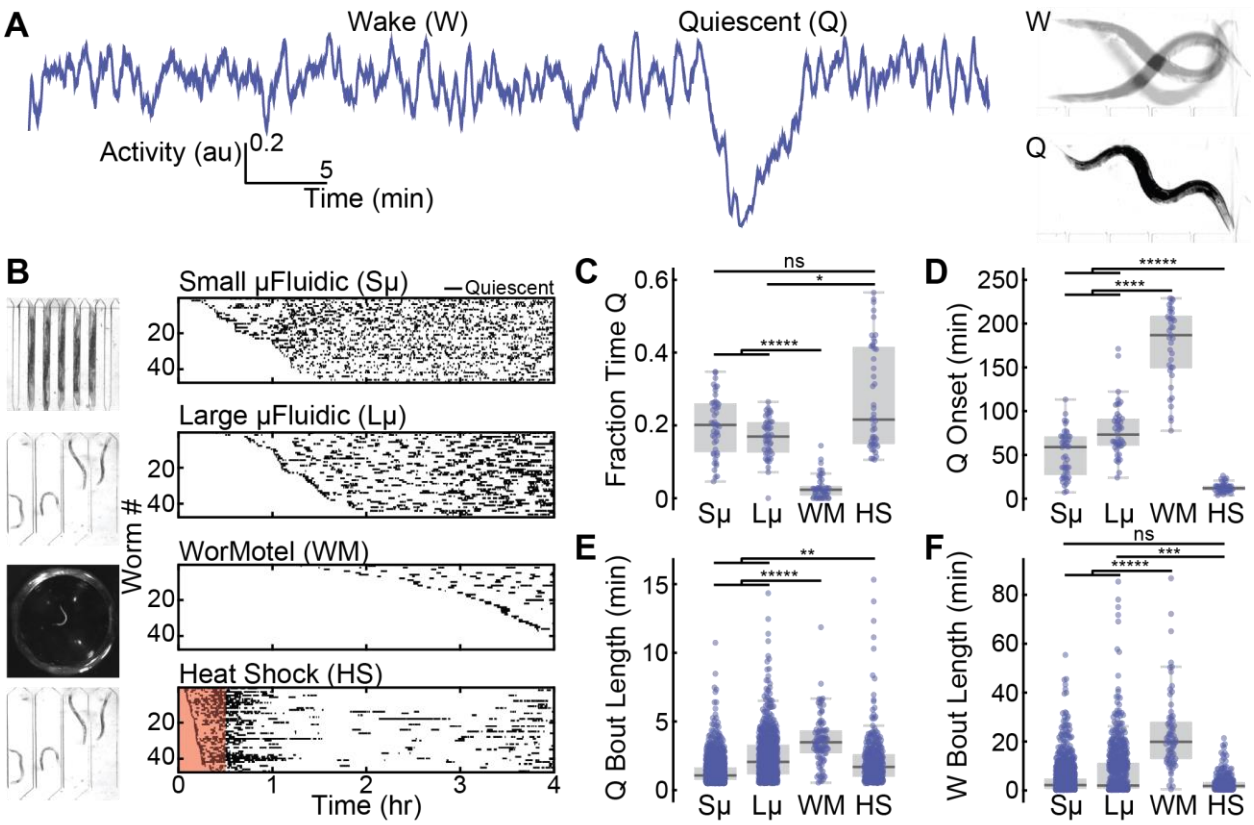

Fig. 1. Microfluidic-induced quiescence is phenotypically distinct from similar *C. elegans* behaviors. *(A)* Characteristic worm quiescence in a microfluidic chamber. *(Left)* 1 hr activity trace from a worm swimming in a microfluidic chamber, calculated by subtracting consecutive frames to quantify movement (see Methods). Quiescence is hallmarked by a clear drop in animal activity to near zero. *(Right)* 1 s overlap of frames shows the animal swimming during the wake period (W) and immobile during quiescence (Q). *(B)* All quiescent bouts recorded from animals in a small microfluidic chamber (50 µm width), large microfluidic chamber (500 µm width), WorMotel multi-well PDMS device, and large microfluidic device during a 30 min heat shock at 30 °C (see inset images). Raster plots show the bouts recorded from each animal during a 4 hr imaging period (n = 47 animals for each condition). Experiments represented in the raster plots are sorted by the onset of the first detected sleep bout. *(C-F)* Quantitative sleep metrics. Sµ = small microfluidic chambers, Lµ = large microfluidic chambers, WM = WorMotel, HS = first hour of heat shock. *(C)* The total fraction of time each animal spent in the quiescent state. *(D)* Onset time of the first quiescent bout. *(E)* Length of individual quiescent bouts. *(F)* Length of individual wake bouts, excluding the first period of wake after animals are loaded into the chamber. (n = 47 animals for each condition; *$p < 0.05$, ** $p < 0.01$, ***$p<0.001$, ****$p<0.0001$, *****$p<0.00001$; Kruskal-Wallis with a *post-hoc* Dunn-Sidak test).

Our observation of spontaneous *C. elegans* quiescence in microfluidic chambers led us to determine whether this behavioral state transition meets the evolutionarily-conserved criteria for classification as sleep: reversibility, a decreased response to stimuli, homeostasis, and a stereotypical posture (24). *C. elegans* developmentally-timed sleep as larvae meets all requirements (25, 26, 46, 57–62). However, sleep in adult worms—which occurs in only specific environmental conditions—is typically defined based on reversibility and a decreased response to stimuli (40, 46). Here, we tested for reversibility, decreased response to stimuli and a micro-homeostatic rebound.

To test for reversibility, we used blue light (5 s pulse, 5 mW/cm^2) as a strong stimulus and found that this rapidly and reliably reversed the quiescent state (Fig. 2A, Movie S3). To test for a decreased response to stimuli, we fabricated microfluidic push-down valves designed to deliver tunable mechanical stimuli, similar to previously developed technology for worms (63). We found that when we applied a strong stimulus (high pressure, 30 psi), both wake and quiescent animals robustly responded with a significant increase in behavioral activity, which provides additional confirmation that the quiescent state is reversible (Fig. 2B, S1, Movie S4). When we applied a weak stimulus to wake animals (low pressure, 15 psi), we again reliably recorded a significant increase in activity (Fig. 2B, S1, Movie S5). However, when we delivered a weak stimulus to quiescent animals, they responded weakly, exhibiting an average behavioral activity less than half that of all other conditions (Fig. 2B-C, S1, Movie S5). These data suggest that during quiescence, sensory systems are less responsive and in a reduced activity state, consistent with previous reports during *C. elegans* sleep (25, 26, 40, 61). In addition, we also tested for homeostatic rebound, which is found in worm developmental sleep (25, 43, 57). Because sleep deprivation produced with external stimuli (e.g. mechanical pulses) can produce a

stress response (58), we tested whether sleep bout length depends on the length of the previous wake bout (Fig. S2). We hypothesized that longer wake bouts would lead to longer sleep bouts due to micro-homeostatic mechanisms, as previously observed for developmental sleep (57). Indeed, we found that sleep bouts increased from 1.5 ± 0.1 min to 2.5 ± 0.1 min (mean ± sem) as the preceding wake bout increased in length from < 1 min to 20 min (Fig. S2). However, even when wake bout lengths increased to longer than an hour, the sleep bouts lengths plateaued to an average of only 2.3 ± 0.1 min (Fig. S2), contradicting the hypothesis that extended wake periods lead to sleep deprivation and homeostatic rebound. These results suggest that micro-homeostasis may be present in μSleep; however, future work is needed to test for homeostatic rebound based on non-stress-inducing sleep deprivation, such as optogenetic inhibition of sleep-promoting neurons (43). Together our results indicate that microfluidic-induced quiescence indeed meets the behavioral precedents to be called a *C. elegans* sleep state: reversibility and a decreased response to stimuli.

To further validate that μSleep is a sleep state, we interrogated the role of two interneurons, RIS and ALA, known to dominate *C. elegans* developmental and stress-induced sleep, respectively, via at least partially distinct signaling pathways (46, 64). To test whether μSleep is also dependent on these neurons, we compared the sleep phenotype of WT, *ceh-17(lf)* and *aptf-1(lf)* loss-of-function mutants (Fig. 2D). *ceh-17(lf)* shows defective axonal growth of the ALA neuron (35) and less stress-induced sleep (40). *aptf-1(lf)* lacks the transcription factor necessary for RIS to signal quiescence via the FLP-11 neuropeptide and shows defects in developmental sleep (38, 39). In our experiments, both *ceh-17(lf)* and *aptf-1(lf)* mutants showed more than 4.5 times less total μSleep than WT animals (Fig. 2E), further validating that μSleep is a *C. elegans* sleep state controlled by previously-reported neural mechanisms.

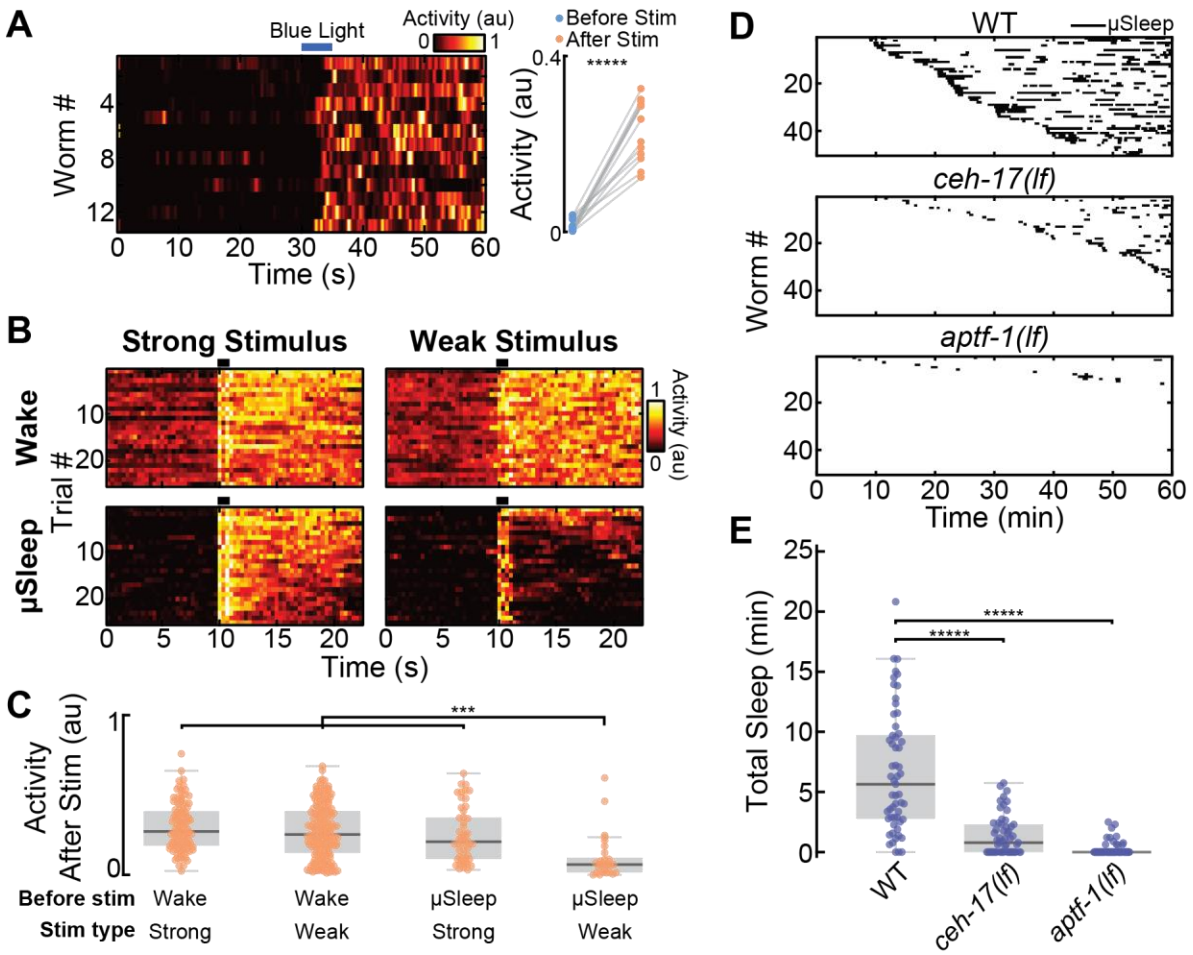

Fig. 2. Microfluidic-induced quiescence is a sleep state. *(A)* The quiescent state is reversible. *(Left)* Heatmap of animal activity. Measurements begin with all animals in the quiescent state. The 5 s light pulse at t = 30 s results in a rapid increase in animal activity. *(Right)* Mean activity of each animal during the first and second 30 s of imaging shows a clear transition from quiescent to wake states (n = 13 worms, *****$p < 0.00001$, paired t-test). *(B)* Quiescent animals have a decreased response to weak sensory stimuli. Heatmaps of activity from wake and quiescent animals that received strong or weak mechanical stimuli from microfluidic valves (Movie S4-S5). For each condition, only the 25 trials with the highest mean activity post-stimulation are shown. "Wake" indicates trials in which animals were awake but have a below-average activity before stimulation (see Methods). "µSleep" indicates trials in which animals were quiescent before stimulation. All conditions show an increase in activity upon stimulation (see Fig. S1), but fewer animals are responsive when receiving weak stimuli. *(C)* Mean activity after mechanical stimulation from the trials in (B). Behavioral activity is identical in all cases other than when quiescent animals received weak mechanical stimuli (Wake-Strong n = 108, Wake-Weak n = 176, µSleep-Strong n = 51, µSleep-Weak n = 29; ***$p < 0.001$, Kruskal-Wallis with a *post-hoc* Dunn-Sidak test). *(D)* Raster plots of detected sleep bouts from WT, *ceh-17(lf)* and *aptf-1(lf)* animals. Only the top 50 animals showing the most total µSleep are shown. *(E)* Both *ceh-17(lf)* and *aptf-1(lf)* show less total sleep than WT. The data suggest that µSleep is strongly dependent on the ALA and RIS neurons (WT n

= 57, *ceh-17(lf)* n = 57, *aptf-1(lf)* n = 60; *****p < 0.00001 compared to WT, Kruskal-Wallis with a *post-hoc* Dunn-Sidak test).

Having established that μSleep meets the criteria for *C. elegans* sleep and is hallmarked by a dramatic behavioral state transition, we also sought to confirm that these spontaneous behavioral transitions were accompanied by an underlying global-brain state transition (33, 65). Previous work in chemically-paralyzed animals used brain-wide calcium imaging to establish that the *C. elegans* nervous system, with the exception of a few neurons, transitions to a large-scale downregulation of neural activity during sleep (33, 65). Yet, this global brain activity has only been observed during *C. elegans* developmental sleep (33) and sleep induced by a 16 hr period of starvation (65), which are both significantly different conditions compared to μSleep. For example, our microfluidic assays use adult animals and we typically observe quiescence within the first hour after removal from food (see Fig. 1, Methods).

Using whole-brain calcium-sensitive imaging we were able to establish that μSleep is indeed associated with a global brain state transition (Fig. 3). For these experiments we found that the μSleep behavior has a distinct advantage compared to other whole-brain imaging experimental preparations. Typically, whole-brain calcium imaging in *C. elegans* exists in two paradigms: volumetric imaging of either freely-moving animals (66–68) or chemically-paralyzed animals confined in microfluidic chambers (32, 33, 65, 69, 70). While imaging freely-moving animals allows for simultaneous quantification of neural activity and behavior, tracking a moving brain during experiments (66, 67) and tracking the location of individual neurons during post-processing (68) remains challenging. Alternatively, chemically paralyzing animals simplifies experiments but does not provide a direct behavioral output during imaging (32, 33, 65, 69, 70). The major advantage of the μSleep behavior for whole-brain imaging is that animals can be confined in microfluidic chambers, which facilitates imaging without the use of paralytics

that could disrupt spontaneous sleep-wake transitions (Fig. 1). To exploit this advantage, we developed an imaging protocol using a microfluidic chamber geometry similar to previous studies (32, 33, 69, 70) that partially-immobilizes animals but allows for enough movement to quantify animal behavior and detect μSleep during whole-brain calcium imaging (Fig. 3). By incorporating a period of animal habituation to blue excitation light, we were able to image continuously for 10 minutes using single-plane epifluorescence microscopy and capture spontaneous sleep-wake transitions in approximately 25% of animals (see Methods). Imaging a single 2D-plane allowed for quantifying both average ganglia activity and the activity of several individual neurons (Fig. 3B, Movie S6-S7). With this imaging protocol, we observed a distinct correlation between animal behavior and neural activity (Fig. 3B, Movie S6-S7). During μSleep both the average ganglia activity and the activity of individual neurons dropped significantly (78 ± 10% and 55 ± 10%, respectively) (Fig. 3C). However, as expected from previous work (33, 38, 39, 43, 65), we observed that some neurons actually increased in activity during μSleep (Fig. 3C). Single-neuron imaging confirmed that the RIS neuron, which has been proposed as a sleep-promoting neuron for multiple *C. elegans* sleep-like states (38, 39, 43), indeed showed more than a two-fold increase in calcium activity during μSleep and strongly correlated with low-behavioral activity (Fig. S3). These results further support the claim that μSleep is a *C. elegans* sleep behavior controlled by sleep-promoting circuits and corroborate previous reports that a unique brain state governs *C. elegans* sleep (33, 65). Furthermore, these results show that μSleep behavior is an advantageous behavioral paradigm that facilitates whole-brain imaging while measuring animal activity without the need for chemically induced paralysis.

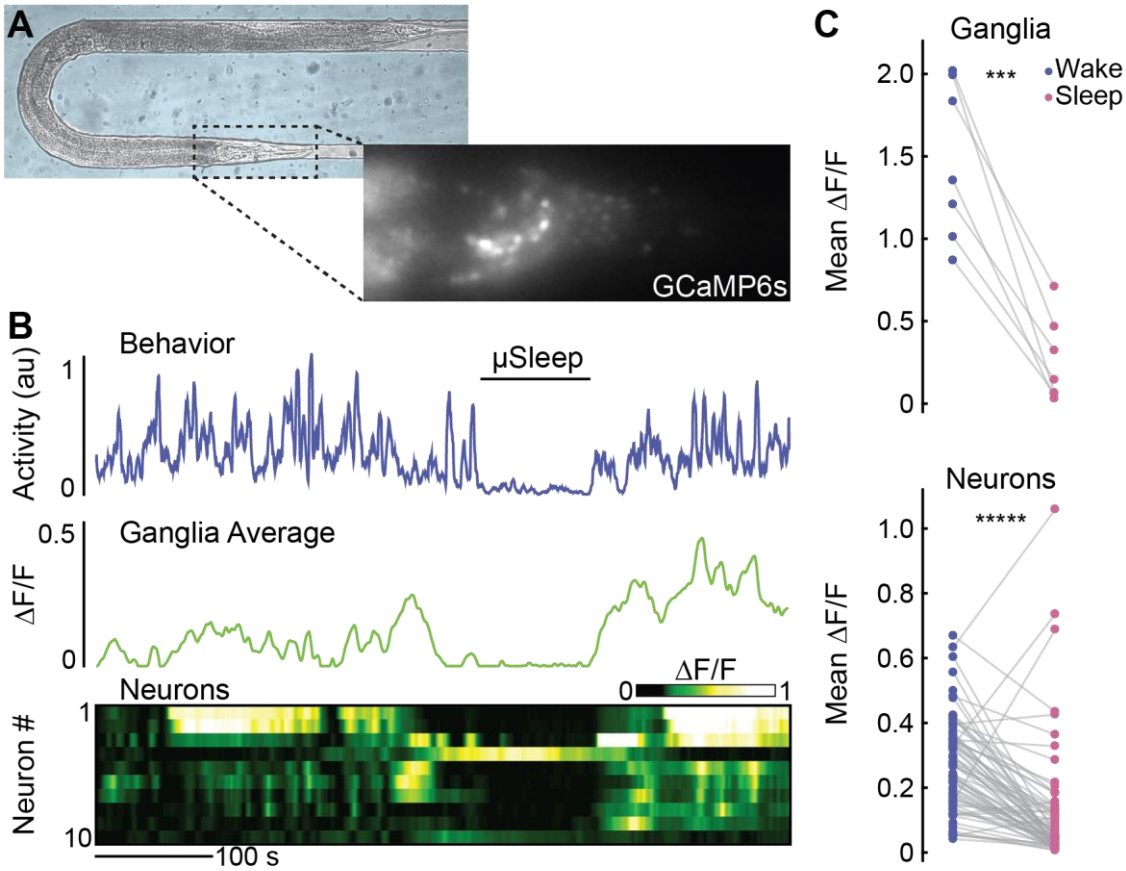

Fig. 3. A global-brain state transition governs *C. elegans* μSleep. *(A)* Adult animal immobilized in a microfluidic chamber tailored for whole-brain imaging. *(Inset)* Single-plane epifluorescence image of an animal with pan-neuronal expression of GCaMP6s. *(B)* Representative animal shows behavioral quiescence correlates with less neural activity. *(Top)* Behavioral activity trace quantified by tracking the motion of ten individual neurons (see Methods). *(Middle)* Average fluorescence across the whole worm head ganglia. *(Bottom)* Activity of ten individual neurons show a clear brain-state transition and less neural activity during μSleep. *(C)* Using only behavioral activity, we identified quiescent bouts then quantified neural activity during sleep and wake. During μSleep, animals exhibited a large-scale downregulation of neural activity across both the entire ganglia and most individual neurons. (n = 7 animals; 10 neurons were tracked per animal; ***$p < 0.001$, *****$p < 0.00001$, paired t-test).

While the combination of behavioral and calcium-imaging data shows that μSleep is hallmarked by a spontaneous brain *and* behavioral state transition (Fig. 3) regulated by sleep-promoting neurons like RIS and ALA (Fig. 2, S3), we also wanted to understand what neural circuits upstream of these neurons are involved in regulating μSleep. Based on our observation of distinct phenotypes when comparing swimming animals in WorMotel to swimming animals in microfluidic chambers (Fig. 1), we hypothesized that *C. elegans* sensory circuits detect features unique to the microfluidic environment and in turn drive sleep behavior. To elucidate the cues regulating μSleep, we used the versatility of microfluidics to perform assays under a variety of conditions and compared the μSleep phenotype to the baseline behavior observed in a large microfluidic device (Fig. 4A). We defined our baseline experimental conditions as: 20 °C cultivation temperature (T_c); animals are transferred directly from seeded nematode growth media (NGM) into the microfluidic device; the microfluidic media (M9 buffer) contains no food source; the temperature during imaging is 22 °C.

We first tested how food availability affects the μSleep phenotype. The presence of food is known to change the swimming-induced quiescence phenotype (52, 53), high quality food induces quiescence (71), and extreme starvation also leads to sleep-wake switching (43, 65). Therefore, we hypothesized that the internal satiety state is a significant regulator of μSleep. To test this hypothesis, we assayed three satiety states in WT animals: “Starved” animals were starved for 2 hr before being loaded into a chambers with no food; “Baseline” animals were loaded directly from a NGM food source to a microfluidic device with no food; and “+Food” animals were loaded from a NGM food source into a microfluidic device with food dissolved in the buffer. As expected, we observed less total μSleep per worm as satiety increased from “Starved” (15 ± 2 min, mean ± sem) to “Baseline” (5.4 ± 0.9 min) to “+Food” (0.4 ± 0.2 min)

(Fig. 4A-B). These results show that satiety is a strong regulator for μSleep, which may have evolved to optimize the tradeoff between energy conservation and the search for food.

Other well-known drivers of sleep are noxious environmental stressors, which we also tested in the context of our microfluidic chambers. Heat shock at temperatures greater than 30 °C is a common method to induce cellular stress and *C. elegans* sleep (34, 40, 44, 45, 54, 72). Although our standard μSleep assays were conducted at only 22 °C, we investigated whether these small changes from T_c could be a possible environmental regulator of quiescence. Indeed, we discovered that increasing the assay temperature to 25 °C, which is still well below commonly used temperatures for heat-shock (30-40 °C), increased the total observed sleep 3.5-fold (Fig. 4A, C). Cooling the device to 18 °C (i.e. below T_c) had the opposite effect and nearly abolished all μSleep bouts (Fig. 4C, S4). To show that these changes in phenotype are mediated by *C. elegans* thermosensation, we tested triple-knock-out *gcy-23(nj37);gcy-8(oy44);gcy-18(nj38)* mutants, which show disruption to thermosensation that is specific to the AFD neurons, the primary temperature-sensing neurons in *C. elegans* (73, 74). In AFD-defective animals we observed no significant change in total μSleep when raising the temperature from 18 °C ("cool") to 22 °C ("baseline"). Under the same conditions WT animals showed a 540-fold increase in total μSleep (Fig. 4C). Furthermore, thermosensory-defective mutants displayed 80% less μSleep at 22 °C ("baseline") and 45% less μSleep at 25 °C ("heat") when compared to WT animals (Fig. 4C, S4). These results suggest that AFD neurons transduce changes in environmental temperature and drive downstream sleep-promoting circuits. These results show that temperature changes significantly less than those typically used for heat shock can dramatically change the μSleep phenotype. In addition, this is the first indication that thermosensory input can act bidirectionally to either promote or suppress *C. elegans* quiescence.

The final environmental factor we investigated was animal confinement. Under baseline conditions, animals swim in large 500 μm-width chambers (Fig. 4D, inset). We found that confining animals to a smaller 110 μm-width chamber, where the primary motion is crawling-like (Fig. 4D inset) leads to the same amount of total μSleep as the baseline chambers (Fig. 4D, S4). However, when we partially compressed WT animals in small 50 μm-width chambers, we observed nearly a 4-fold increase in total sleep compared to baseline (Fig. A, D, S4). We hypothesized that this change in phenotype due to immobilization was at least partially mediated by mechanosensory circuits. For example previous reports showed that touch-defective mutants *mec-10(tm1552)* have a decreased ability to sense spatial patterns in microfluidic arenas (75). We tested *mec-10(tm1552)* as well and found that when minimal mechanical stress was present (i.e. 500 μm and 110 μm width chambers), total μSleep remained insignificantly unchanged compared to WT (Fig. 4D, S4). However, when *mec-10(tm1552)* animals were compressed, total animal μSleep decreased by a factor of two compared to WT animals under the same conditions (Fig. 4D, S4), indicating that mechanosensory pathways are necessary for restraint-induced μSleep. In addition, we also tested *mec-4(e1611)* mutants, which are defective in response to gentle touch, but remain sensitive to harsh touch (76). These animals showed no significant difference in total μSleep compared to WT when immobilized (Fig. S5), indicating that nociceptive mechanosensory pathways are required to drive μSleep. Together, these results show for the first time that *C. elegans* microfluidic immobilization induces sleep behavior through harsh mechanosensory pathways.

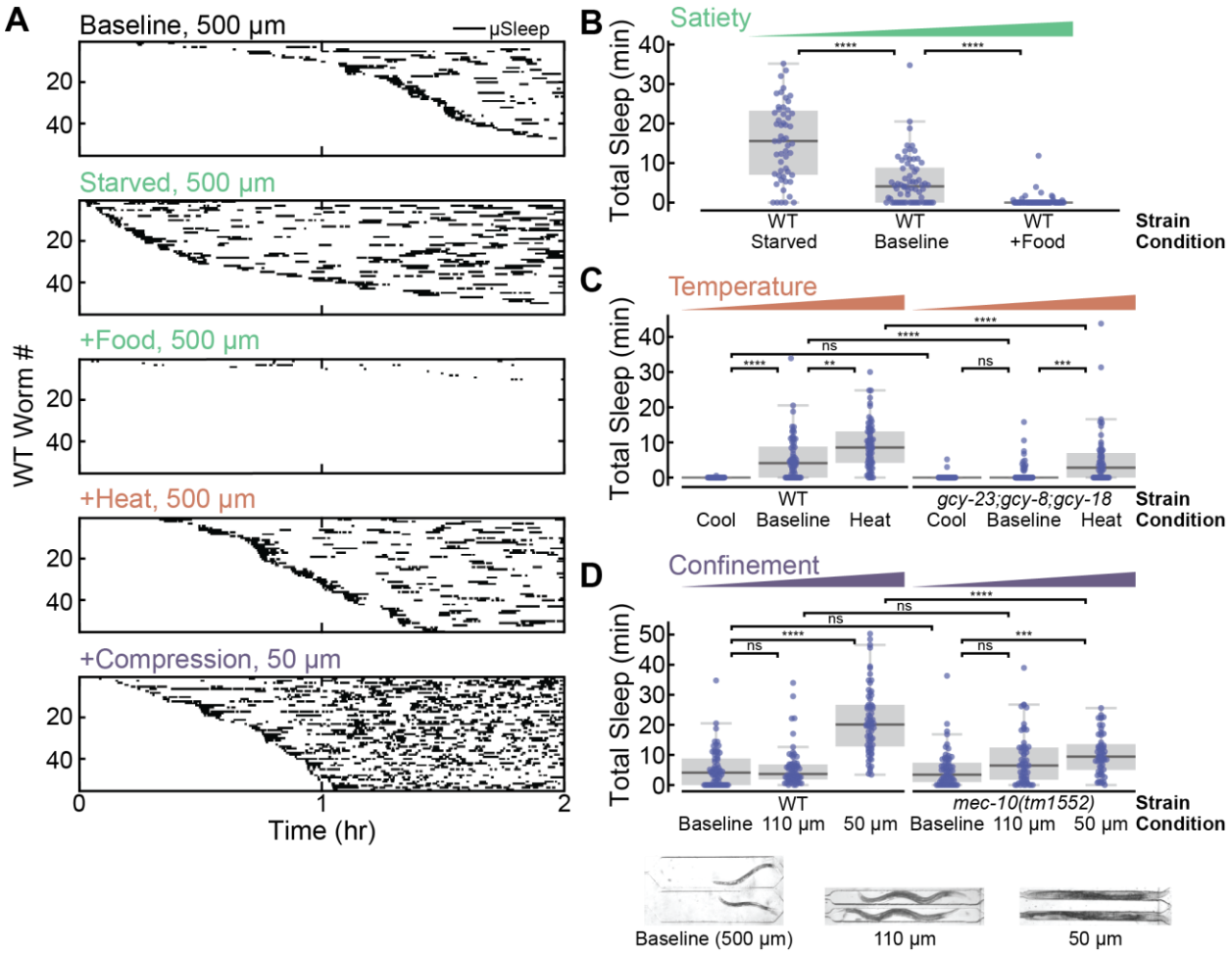

Fig. 4. µSleep is regulated by satiety and multiple sensory circuits. *(A)* Detected sleep bouts for WT animals in several experimental conditions. Raster plots show detected sleep bouts during a 2 hr imaging period. "Baseline" indicates the standard experimental conditions. "Starved" indicates animals that were starved prior to the assay. "+Food" indicates conditions in which *E. coli* OP50 was added into the buffer during recordings. "+Heat" indicates imaging conditions where the temperature was raised to 25 °C. "+Compression" indicates that animals are partially immobilized in 50 µm-wide chambers. See micrographs under (D) for chamber geometries. In all cases, the sleep phenotype varies dramatically from the baseline. Only the 55 animals that displayed the most sleep are plotted for clarity. Raster plots for all WT and mutant animals are shown in Fig. S4. *(B)* Total WT sleep under varying satiety conditions. As satiety increases from "Starved" to "+Food," animals exhibit less µSleep (from left to right on the plot the number of animals n = 55, 68, 67). *(C)* Total µSleep under varying temperature conditions. "Cool" = 18 °C, "Baseline" = 22 °C, "Heat" = 25 °C. Increasing temperature increases total µSleep for WT animals. Thermosensory-defective mutants show the same µSleep phenotype as WT at 18 °C, but significantly less sleep as 22 °C and 25 °C, indicating that thermosensory input can act to drive or suppress µSleep (from left to right on the plot the number of animals n = 37, 68, 71, 41, 67, 60) *(D)* Total sleep under different confinement conditions. Micrographs show chamber geometries. When WT animals are confined in smaller chambers, they only show an increase in total µSleep when slightly compressed in 50 µm-wide chambers. *mec-10(tm1552)* mutants show an identical phenotype to WT in 500 µm and 110 µm chambers, but dramatically reduced sleep compared to WT when compressed. These

results suggest that nociceptive input to mechanosensory neurons regulates μSleep (from left to right on the plot the number of animals n = 68, 64, 69, 66, 64, 57). (ns = not significant, ** $p < 0.01$, ***$p<0.001$, ****$p < 0.0001$; Kruskal-Wallis with a *post-hoc* Dunn-Sidak test).

Given the dependence of μSleep on satiety, temperature, and mechanical stress (Fig. 4), we hypothesized that each of these factors could act as stressors that contribute to a slow-onset form of stress-induced sleep. Previously, studies of stress-induced sleep in *C. elegans* have reported acute and rapid sleep responses to noxious external stimuli (34, 40, 44, 45, 54, 72), leading us to investigate if the slow-onset μSleep state could be weaker form of stress-induced sleep. To test this hypothesis, we assayed DAF-16::GFP animals in the identical environmental conditions shown in Fig. 4. The Fork head transcription factor DAF-16 regulates longevity, metabolism, and some stress responses in *C. elegans* (77–79). While normally diffuse in the cytoplasm, under unfavorable environmental conditions (e.g. heat shock), DAF-16::GFP localizes to the nucleus (79). Thus DAF-16::GFP puncta formation can serve as a proxy for *C. elegans* stress under some conditions (note that some noxious conditions, such as UV exposure do not lead to DAF-16 aggregation (79)). We quantified puncta formation in different environmental conditions and observed that DAF-16::GFP localization correlated with μSleep phenotypes in only some cases (Fig. S6). We found that compared to Baseline animals, +Heat animals showed greater than a 250% increase in the number of cumulative puncta and +Food animals showed almost zero puncta formation (Fig. S6), which is in agreement with previous reports of stress responses (79, 80), These results support the hypothesis that 25 °C and the lack of food in the microfluidic devices increases animal stress and upregulates μSleep. However, +Cool animals, which showed almost zero μSleep bouts (Fig. 4), surprisingly displayed a 2X increase in cumulative puncta compared to Baseline animals (Fig. S6). In addition, +Compression animals showed no significant difference in the number of DAF-16 puncta

compared to Baseline (Fig. S6), despite displaying dramatically more total μSleep (Fig. 4). These results suggest that animal stress may not completely explain the changes in μSleep we observe during environmental manipulations.

In addition to environmental elements like mechanical compression and temperature that change sleep, we ruled out the possibility that O_2 depletion, CO_2 buildup, or the buildup of other unknown substances dramatically affect μSleep (Fig. S7). To rule out these factors we used replaced the static buffers (used for Fig. 1-4) with a constantly replenished buffer using a gentle buffer flow that is expected to stabilize gas concentration levels and remove any animal byproducts. Surprisingly, we observed that the gentle flow led to more sleep (Fig. S7). Therefore, a lack of O_2 or a buildup or CO_2 are not major drivers of μSleep.

Environmental changes, particularly to the chamber geometry also led to phenotypic changes not captured by quantifying total μSleep (Fig. 4). For example, WT animals in 110 μm chambers showed an accelerated onset of sleep bouts (Fig. S4), but bouts were shortened, leading to overall the same amount of μSleep as WT in 500 μm chambers (Fig. 4). Future work will continue to interrogate how sensory mechanisms regulate sleep and arousal. Overall, our environmental manipulations conclusively show that the animal satiety state, the mechanical environment, and the local temperature strongly regulate the μSleep phenotype. Thus, μSleep is a multisensory-regulated sleep behavior that is also strongly modulated by internal physiological factors.

Discussion:

Here, we described a spontaneous *C. elegans* brain and behavioral state transition that is unique to microfluidic chambers, which facilitates whole-brain imaging and precise regulation of

the environment. μSleep regulation appears to be at least partially linked to a slow-onset form of stress-induced sleep (Fig. S6), and may also be related to swimming-induced quiescence (49, 51, 52). Despite these potential similarities, the behavioral phenotype we measured is quantitatively distinct from these previously reported worm quiescent behaviors (Fig. 1). We showed that μSleep is reversible (Fig. 2A), that animals exhibit a decreased response to sensory stimuli while quiescent (Fig. 2B-C, S1), and that quiescence is dependent on known *C. elegans* sleep-promoting neurons, ALA and RIS (Fig. 2D-E). Thus, μSleep meets the precedent set for worm sleep behavior (40, 46). While we observed a micro-homeostatic rebound when animals exhibited long bouts of swimming (Fig. S2), more work is needed to understand whether μSleep is governed by a homeostatic process, perhaps by using optogenetic silencing of RIS neurons for sleep deprivation (43). In addition, we found that thermosensory input via the AFD neuron acts as a bidirectional controller of sleep; cooler temperatures promote wake, while warmers temperatures promote sleep (Fig. 4). Furthermore, we showed for the first time that animal restraint can act through mechanosensory pathways to drive sleep behavior (Fig. 4). Finally, a dramatic brain-state transitions and global downregulation of neural activity, with the exception of a few neurons, underlies μSleep behavioral transitions (Fig. 3).

Though we observe μSleep in the context of microfluidic confinement, it is not hard to imagine that *C. elegans* may use this behavior and downregulation of neural activity in its natural environment. One unifying hypothesis for *C. elegans* μSleep regulation could be rooted in energy conservation. Factors that decreased μSleep, such as food and cooler temperatures, may indicate favorable conditions for active roaming behavior. Conversely, factors that increased μSleep, such as elevated temperatures and animal restraint, may indicate more harmful environments in which roaming and expending energy is not an optimal survival strategy.

Furthermore, the changes we made to the environment may change the animal's metabolic state. *C. elegans* metabolism is known to increase with increasing temperature (81). Additionally, one can imagine that microfluidic immobilization (Fig. 4) drives an escape response, leading to increased muscle activation and high energy expenditure. Therefore, it is possible that all changes in μSleep phenotypes we observed were rooted in optimizing energy use by balancing the between tradeoff between expending energy to move and the expected value of finding food. Future work is needed to continue to elucidate these mechanisms using genetic mutants, different culture conditions, and combining sensory stimuli with food availability. Overall, the ability to control food availability, temperature, and mechanosensory feedback provides a valuable platform to study how quiescent behavior may serve as an evolutionary advantage and successful survival strategy.

Many questions remain with respect to *C. elegans* sleep and how the worm nervous system controls these dramatic state transitions. Sleep-promoting neurons drive behavioral quiescence, but what ensemble activity occurs upstream of these circuits? How are multiple sensory inputs integrated within the nervous system to regulate sleep? How does multisensory integration combine with neuromodulation by the physiological state to control sleep? We envision μSleep platform described here could help researchers interrogate the biological principles that regulate brain and behavioral state transitions and investigate how these principles adapt in changing environments and physiological states. These studies are made possible by the combination of whole-brain imaging and behavioral recordings with simultaneous control of the microfluidic environment. Future opportunities include volumetric whole-brain imaging (66–68) that could capture the activity of nearly every neuron in the worm brain to elucidate how ensemble activity drives state transitions. Combining these imaging methods with high-

throughput microfluidic assays and dynamic environmental control will lead to a large library of simultaneous behavioral and brain-wide data under many experimental conditions. These data, combined with computational techniques, would provide a rich resource to understand how many circuits across the *C. elegans* nervous system regulate brain- and behavioral states.

Materials and Methods:

C. elegans Strains and Maintenance

All strains were maintained at 20 °C on standard Nematode Growth Medium (NGM) seeded with *E. coli* OP50 as the food source. All experiments were performed with day-1 adult animals. The strains used for each experiment are as follows

Fig. 1: N2

Fig. 2: N2, IB16 *ceh-17(np1)* I; HBR227 *aptf-1(gk794)* II

Fig. 3: AML32 (*wtfIs5 [prab-3::NLS::GCaMP6s; prab-3::NLS::tagRFP]*)

Fig. 4: N2, IK597 *gcy-23(nj37);gcy-8(oy44);gcy-18(nj38)* IV, ZB2551 *mec-10(tm1552)*

Fig. S1: N2

Fig. S2: N2

Fig. S3: HRB1361 (*goeIs304[pflp-11::SL1-GCaMP3.35-SL2::mKate2-unc-54-3'UTR, unc-119(+)]*)

Fig. S4: N2, IK597 *gcy-23(nj37);gcy-8(oy44);gcy-18(nj38)* IV, ZB2551 *mec-10(tm1552)*

Fig. S5: N2, CB1611 *mec-4(e1611)*

Fig. S6: TJ356 (*zIs356 [daf-16p::daf-16a/b::GFP + rol-6(su1006)]*)

Fig. S7: N2.

Microfluidic Device Fabrication

Standard photo- and soft-lithography techniques were used to fabricate microfluidic devices (82). Microfluidic geometries were custom designed in CAD software. Most photomasks were transparencies (CAD/Art Services Inc.), but glass photomasks (Front Range Photomask) were used for higher-resolution devices (Fig. 3, S7). All master molds were fabricated using SU-8 2075 (MicroChem). The SU-8 height for worm behavioral channels was 75 μm (spin: 20 s – 500 rpm, 30 s – 3000 rpm), but we used a height of 50 μm (spin: 20 s – 500 rpm, 30 s – 4000 rpm) for whole-brain imaging devices to further constrict animal movement. We used polydimethylsiloxane (PDMS) Sylgard for all microfluidic chips. All behavioral chips were double-layer devices to incorporate push-down valves for sealing the chamber entrances or delivering mechanical stimuli. The bottom worm layer (20:1 ratio, spin: 930 rpm for 30s) was bonded to the upper valve layer (10:1 ratio) using a 30 s exposure to oxygen plasma (200 W, 330 mTorr), then baked together for at least 12 hr. The PDMS devices were permanently bonded to either a standard glass slide for behavior, or a 300 μm-thick quartz wafer (NOVA Electronics Materials) for whole-brain imaging.

Behavioral Quantification and Sleep Detection

To quantify *C. elegans* activity, we used the previously described method of frame-by-frame subtraction (83). This method subtracts consecutive frames from one another, then counts the number of pixels that substantially change value. Worm movement leads to a large number of pixels that change from frame-to-frame. Quiescent animals, which move very little, lead to few pixels that change values from frame-to-frame. We performed frame-by-frame subtraction, drew regions-of-interest around each animal, then counted the number of pixels in the ROI that

changed by a value greater than 30 (a number well above the noise level of the CMOS sensor). This yields a raw activity trace for each animal. We also used standardized methods to normalize activity traces (52, 53), which accounts for changes in brightness across the field-of-view (FOV), and allowed us to set a consistent sleep detection threshold across populations. In most cases, we smoothed activity traces across 20 s, then normalized to the top 95th percentile, yielding a normalized activity trace for each animal with values approximately between 0 and 1. For analysis that required finer timescales on the order of less than 20 s (Fig. 2 A-C), we did not smooth activity traces (see "Reversibility and Decreased Response to Stimuli" subsection).

Once we normalized the activity trace, we thresholded the data to detect sleep. The threshold depended on the microfluidic geometry. For example, in large microfluidic chambers (Movie S1), movement could still be detected during μSleep as animals drifted across the chamber. In smaller microfluidic geometries (Movie S2), worm activity was already significantly constrained, so a stricter threshold was needed to detect sleep. We determined thresholds by manually scoring 20 sleep bouts, calculating the mean activity during those bouts, then doubling the mean activity. The thresholds used for each geometry were: WorMotel – 0.15; 500 μm microfluidic chambers – 0.15; 110 μm microfluidic chambers – 0.08; 50 μm chambers – 0.06. A minimum sleep bout time of 30 s was used to reduce false detections. In addition, during a sleep state brief animal twitching lasting less than 15 s was not counted as a wake period.

Standard Microfluidic Behavioral Assays

Unless otherwise stated, behavioral assays took place on an enclosed AmScope SM-2T-LED stereo microscope. Red transparency was used to filter out LED wavelengths that potentially affect animal behavior. Imaging was performed at 3 fps with either a Point Grey Grasshopper (GS3-U3-23S6M-C) or Basler Ace (acA1920-40um) CMOS cameras, which have nearly identical sensor specifications. While the experiments were typically carried out in a room held at 20 °C, the heat from the LED raised the microfluidic device temperature to 21-22 °C (the "Baseline" temperature in Fig. 4).

M9 buffer was used for all experiments, with no food added unless otherwise stated. During standard experimental conditions, we used a hair pick to transfer day-1 adults directly from seeded NGM into the buffer of an open syringe cap. We then suctioned animals into Tygon tubing that led to the microfluidic chambers. The process of loading 6-12 animals into the chambers (depending on the geometry used) typically took less than 5 min. A push-down valve closed off the entrance of all worm chambers to prevent animals from escaping during imaging. After use each day, devices were flushed with ~6 mL of DI water, sonicated for 10 min, flushed again with DI water, boiled for 15 min, and flushed a final time before storage at ~80 °C overnight.

WorMotel Assays

A 48-well WorMotel molded from PDMS was provided by the Fang-Yen Lab (56). Only 12 wells were used simultaneously. Prior to use, the PDMS was exposed to oxygen plasma for 30 s to make the surface hydrophilic. Each well was then filled with 8 μL of M9 buffer. Using a hair pick, we removed individual animals from seeded NGM, washed them in an M9 droplet, then transferred them into the WorMotel wells. For imaging, the PDMS was inverted and reversibly sealed on a glass slide during imaging (see Churgin *et al.* 2017). The glass slide was treated with Rain-X to prevent condensation. The device was illuminated obliquely with three AmScope Goose-neck LEDs that were filtered with red transparency. As with microfluidic devices, the

temperature during imaging was 21-22 C. We imaged from below at 3 fps with a Point Grey Grasshopper (GS3-U3-23S6M-C).

Heat-Shock

Device setup and animal loading was performed as previously stated (see Standard Microfluidic Behavioral Assays subsection). However, the device was preheated to 30 °C with two Peltier heaters placed on each side of the glass slide. Heat was applied for the initial 30 min of imaging, after which the current through the Peltier heaters was reversed such that the device was rapidly brought to the standard 22 °C. This heat-shock protocol was adapted from that used for agar plates in Hill *et al.* 2014.

Reversibility and Decreased Response to Stimuli

Reversibility assays were conducted on an inverted Nikon microscope and performed with 50 μm-wide microfluidic chambers (Movie S3). Animals were loaded into the chambers and left for 30 min. Between 30 and 60 min, upon visual confirmation of sleep, we initiated a protocol of 60 s of imaging at 10 fps. At 30 s, a strong light stimulus (460 nm light at 5 mW/mm^2) was presented for 5 s to awaken animals. Only animals that were asleep for the full 30 s prior to the light stimulus were kept for analysis.

To test for a decreased response to stimuli, we fabricated 110 x 1100 um microfluidic chambers to confine animals (Movie S4-S5). In addition to the push-down valve used to keep animals in each chamber, we incorporated two push-down valves used for mechanical stimulation. The two valves ensured that animals were almost always in contact with at least one valve during pressurization. For strong and weak stimulation we used a valve pressure of 30 and 15 psi, respectively. 7 groups of animals were used for weak stimulation and 4 for strong stimulation; each group consisted of 8-12 animals. During the hour-long assay, animals received a 0.5 s valve pulse every 3 min. During post-processing, we analyzed animal activity around each stimulation timepoint. For the 10 s prior to each stimulation timepoint, we classified animals as quiescent, slow-moving, or fast-moving. Two categories for wake behavior (i.e. slow-moving and fast-moving) were necessary because a behavioral response could not be detected in animals that were already moving with a high activity. That is, an animal that was clearly awake and moving with high activity in the microfluidic chamber did not display increased activity after receiving mechanical stimuli. However, a detectable behavioral response was apparent in wake, but low-activity animals. We used an activity threshold of < 0.08 for quiescent animals, 0.08-0.35 for low-activity animals, and > 0.35 for high-activity animals (the average animal activity across all traces was 0.36). This classification was performed for each stimulation (20 stimulations for each animal). After classifying animals into each group, we also calculated the mean activity for 10 s post-stimulation, excluding a 2 s period where the microfluidic valves caused movement artifacts. The pre- and post-stimulation activities for quiescent and low-activity comprise the data shown in Fig. 2 and S1.

Whole-Brain Imaging

Microfluidic devices were fabricated as previously described (see “Microfluidic Device Fabrication” subsection), and geometries were modeled off of previous methods for whole-brain imaging (32, 33, 65, 69, 70); however, animals were not chemically paralyzed. We used transgenic animals with pan-neuronal expression of GCaMP6s in the nuclei of all neurons (66, 68). Experiments were performed on an inverted Nikon microscope with a 40X water-immersion

objective (NA = 1.15). An Andor Zyla 4.2 USB 3.0 sCMOS captured the images at 5 fps (50 ms exposures, 2x2 binning). Because blue light can wake *C. elegans*, when animals were immobilized in the chambers, we first initialized a "habituation" protocol. Here, we flashed the 460 nm excitation light for 0.15 s at 1 Hz for 30 min. This habituated animals without photobleaching the calcium indicator. After the habituation period, we imaged continuously for 15 min, but only analyzed the first 10 min of data due to photobleaching. With this protocol, we captured a sleep-wake transition in ~25% of animals.

To analyze data, we chose 10 neurons at random to track by hand in ImageJ. An 8x8 pixel ROI was then used for each neuron in each frame. A neuron near the center of the ganglia was used to draw an ROI around the head ganglia to calculate average brain fluorescence in each frame. We calculated animal activity in two ways: by frame-by-frame subtraction (sampling the frames a 3 Hz), and by calculating the average displacement of the tracked neurons (Fig. 3, Movie S6). Both methods were prone to fluctuating baselines that were not present during behavioral-only recordings, making it difficult to set a standard threshold across animals. However, clear quiescent periods were subjectively apparent. Therefore, for each animal we plotted only the animal behavioral activity and selected sleep bouts manually. As before, only bouts longer than 30 s were counted. We then calculated the mean ganglia and neuron fluorescence during sleep and wake for each worm.

Behavioral activity was smoothed over 3 s and normalized as previously described (see "Behavioral Quantification and Sleep Detection" subsection). Raw ganglia and neuron activity was smoothed over 3 s before calculating $\Delta F/F$. We denote $\Delta F/F$ as $[F(t) - F_0(t)]/F_0(t)$ where $F_0(t)$ is the minimum fluorescence value up to time *t*.

RIS Imaging

7-10 animals per trial (6 trials total) were confined and imaged simultaneously under 10X magnification in the 50 μm-wide chamber geometry. HRB1361 animals expressed both GCaMP3 and mKate in RIS neurons under the FLP-11 promoter. Experiments took place on an inverted Nikon microscope, with dual excitation and emission for simultaneous two-color imaging (FF01-468/553-25 and F01-512/630-25 BrightLine dual-band bandpass filters for excitation and emission, respectively). An X-Cite XLED1 light source provided both 460 nm and 565 nm excitation light and a Tucam image splitter (Andor) split the mKate and GCaMP channels onto two Andor Zyla 4.2 CMOS cameras. We imaged animals for 2 hr and used a data-acquisition box (National Instruments) controlled with custom Matlab scripts to simultaneously trigger 10 ms camera exposures and 30 ms XLED flashes at 0.5 Hz (3x3 binning). Following experiments, we flushed animals from the device and recorded the background for each color channel.

For post-processing, we used the mKate channel to quantify behavior and track the location of RIS neurons. After subtracting background, we calculated animal activity by drawing an ROI around each animal and performing the same frame-by-frame subtraction method as previously described (see "Behavioral Quantification and Sleep Detection" subsection), but here we used a with a pixel change threshold of 400 because of the high dynamic range of the Zyla sensor. After normalizing behavioral activity, a threshold of 0.2 was used to detect sleep bouts, with a minimum sleep time of 60 s. To detect the RIS location in each frame, we again subtracted the image background. We then isolated and binarized each animal ROI, leaving only the RIS neuron and, occasionally, pieces of its processes. The largest object in the ROI was the RIS

soma, which we used to attain the soma centroid. To get the average RIS fluorescence in the frame, we drew a 25x25 pixel ROI around the centroid in each channel and averaged the 20 largest pixel values. We normalized this raw fluorescence in each channel by calculating $\Delta F/F = [F(t) - F_0(t)]/F_0(t)$, where $F_0(t)$ is the minimum fluorescence value up to time *t*. Following this normalization, we calculated the ratio of each color channel $R = (\Delta F/F)_{GCaMP}/(\Delta F/F)_{mKate}$. Finally, the reported ratio values are $\Delta R/R = [R(t) - R_o]/R_o$, where R_o is the lower 20th percentile value.

Environmental Control

The microfluidic setup during environmental manipulation was identical the previously stated (see "Standard Microfluidic Behavioral Assays" subsection); however, for each condition we manipulated individual aspects of the environment.

The baseline phenotype in 500 µm-wide chambers (Movie S1, Fig. 4) was chosen because animals could move freely in a manner similar to swimming, thereby reducing the overall effect of the microfluidic confinement.

Most assays involved transferring animals directly from seeded NGM into the microfluidic device. However, under "Starved" conditions we used a hair pick to remove animals from seeded NGM, washed them in a droplet of M9 buffer, then placed them onto a fresh, unseeded NGM plate. After 2 hr, animals were loaded into the microfluidic device with no food in the buffer. Therefore, animals were deprived of a food source for 2 hr when imaging began and did not have access to food during the experiment.

Most assays were also performed with no food in the M9 buffer. However, under "+Food" conditions, we dissolved 4.56 mg/mL of freeze-dried OP50 (LabTie) into the M9 buffer, providing a food source for animals throughout the imaging time.

In "+Compression" conditions, animals were confined to 50 x 1100 um-wide microfluidic chambers (Fig. 4, Movie S2).

As previously stated, the standard imaging temperature due to LED lighting was 21-22 °C (see "Standard Microfluidic Behavioral Assays" subsection). We controlled temperature in the same manner as heat-shock experiments, using Peltier devices to heat or cool the microfluidic chips to 24-25 °C or 17-18 °C, respectively.

DAF-16::GFP Imaging

Experiments took place over the course of 2 hr on Nikon inverted scope with an Andor Zyla 4.2 USB 3.0 sCMOS and 4X magnification for multi-worm imaging. Environmental control took place as described in the "Environmental Control" subsection. Every 5 min, we captured 7 frames (20 ms exposures) at 1 Hz with 1x1 binning. Otherwise, animals were in darkness. Following imaging, we flushed animals from the chamber and recorded background frames.

Puncta quantification took place similar to previous methods (80). We subtracted the background from each frame and smoothed the image with a median filter. We thresholded this image to detect animal bodies and drew a ROI around each. The smoothed image was further processed with a 3x3 high frequency filter, which enhanced the contrast of puncta and allowed us to binarize the image to detect most DAF-16 aggregations in the frame. For each animal ROI, we then found puncta by counting all objects with a size between 2 and 30 pixels. To mitigate the effects of animal movement, which caused some animals to appear blurred and reduced puncta

count, of the 7 frames that were captured every 5 min, we averaged the 3 largest puncta counts for each ROI. This average makes up the final puncta count for each animal at the given timepoint. The puncta count reported (Fig. S6) are likely lower than the true count that would be attained with high-magnification imaging. Low-magnification not only increases the number of animals imaged per trial but was also necessary to capture the full length of the large microfluidic chambers. Because we applied the same algorithm to all environmental conditions, we expect the reported trends to remain true in high-magnification conditions.

Acknowledgments:

We thank the Fang-Yen lab for providing the WorMotel device. Henrik Bringmann provided the HRB1361 strain for RIS imaging. We thank Anne Hart, David Raizen and Henrik Bringmann for helpful discussions. Several strains were provided by the CGC, which is funded by NIH Office of Research Infrastructure Programs (P40 OD010440). D.L.G. is funded by the National Science Foundation (NSF) Graduate Research Fellowship Program 0940902 and a training fellowship from the Keck Center of the Gulf Coast Consortia on the NSF IGERT: Neuroengineering from Cells to Systems 1250104. D.L.G. and J.Z. are funded by the Smalley-Curl Institute's Student Training for Advising Research program. We also thank the Rice Shared Equipment Authority where devices were fabricated.

References:

1. Van Atteveldt N, Murray MM, Thut G, Schroeder CE (2014) Multisensory integration: Flexible use of general operations. *Neuron*. doi:10.1016/j.neuron.2014.02.044.

2. Fetsch CR, Deangelis GC, Angelaki DE (2013) Bridging the gap between theories of sensory cue integration and the physiology of multisensory neurons. *Nat Rev Neurosci*. doi:10.1038/nrn3503.

3. Clark DA, Freifeld L, Clandinin TR (2013) Mapping and Cracking Sensorimotor Circuits in Genetic Model Organisms. *Neuron*. doi:10.1016/j.neuron.2013.05.006.

4. Crochet S, Lee SH, Petersen CCH (2018) Neural Circuits for Goal-Directed Sensorimotor Transformations. *Trends Neurosci*. doi:10.1016/j.tins.2018.08.011.

5. Tye KM (2018) Neural Circuit Motifs in Valence Processing. *Neuron* 100(2):436–452.

6. Anderson DJ (2016) Circuit modules linking internal states and social behaviour in flies

and mice. *Nat Rev Neurosci*. doi:10.1038/nrn.2016.125.

7. Marder E (2012) Neuromodulation of Neuronal Circuits: Back to the Future. *Neuron*. doi:10.1016/j.neuron.2012.09.010.

8. Bargmann CI, Marder E (2013) From the connectome to brain function. *Nat Methods*. doi:10.1038/nmeth.2451.

9. McGinley MJ, et al. (2015) Waking State: Rapid Variations Modulate Neural and Behavioral Responses. *Neuron*. doi:10.1016/j.neuron.2015.09.012.

10. McGinley MJ, David S V., McCormick DA (2015) Cortical Membrane Potential Signature of Optimal States for Sensory Signal Detection. *Neuron*. doi:10.1016/j.neuron.2015.05.038.

11. Cohn R, Morantte I, Ruta V (2015) Coordinated and Compartmentalized Neuromodulation Shapes Sensory Processing in Drosophila. *Cell*. doi:10.1016/j.cell.2015.11.019.

12. Bennett C, Arroyo S, Hestrin S (2013) Subthreshold mechanisms underlying state-dependent modulation of visual responses. *Neuron*. doi:10.1016/j.neuron.2013.08.007.

13. Lim RS, Eyjólfsdóttir E, Shin E, Perona P, Anderson DJ (2014) How food controls aggression in Drosophila. *PLoS One*. doi:10.1371/journal.pone.0105626.

14. Talsma D, Senkowski D, Soto-Faraco S, Woldorff MG (2010) The multifaceted interplay between attention and multisensory integration. *Trends Cogn Sci*. doi:10.1016/j.tics.2010.06.008.

15. Adolphs R, Anderson D (2013) Social and emotional neuroscience. *Curr Opin Neurobiol*.

doi:10.1016/j.conb.2013.04.011.

16. Ghosh DD, Nitabach MN, Zhang Y, Harris G (2017) Multisensory integration in C. elegans. *Curr Opin Neurobiol*. doi:10.1016/j.conb.2017.01.005.

17. Calhoun AJ, Murthy M (2017) Quantifying behavior to solve sensorimotor transformations: advances from worms and flies. *Curr Opin Neurobiol*. doi:10.1016/j.conb.2017.08.006.

18. Huston SJ, Jayaraman V (2011) Studying sensorimotor integration in insects. *Curr Opin Neurobiol*. doi:10.1016/j.conb.2011.05.030.

19. Kaplan HS, Nichols ALA, Zimmer M (2018) Sensorimotor integration in Caenorhabditis elegans: A reappraisal towards dynamic and distributed computations. *Philos Trans R Soc B Biol Sci*. doi:10.1098/rstb.2017.0371.

20. Griffith LC (2013) Neuromodulatory control of sleep in Drosophila melanogaster: Integration of competing and complementary behaviors. *Curr Opin Neurobiol*. doi:10.1016/j.conb.2013.05.003.

21. Watanabe K, et al. (2017) A Circuit Node that Integrates Convergent Input from Neuromodulatory and Social Behavior-Promoting Neurons to Control Aggression in Drosophila. *Neuron*. doi:10.1016/j.neuron.2017.08.017.

22. Saper CB, Fuller PM, Pedersen NP, Lu J, Scammell TE (2010) Sleep State Switching. *Neuron* 68(6):1023–1042.

23. Brown RE, Basheer R, McKenna JT, Strecker RE, McCarley RW (2012) Control of Sleep and Wakefulness. *Physiol Rev*. doi:10.1152/physrev.00032.2011.

24. Campbell SS, Tobler I (1984) Animal sleep: A review of sleep duration across phylogeny. *Neurosci Biobehav Rev*. doi:10.1016/0149-7634(84)90054-X.

25. Raizen DM, et al. (2008) Lethargus is a Caenorhabditis elegans sleep-like state. *Nature* 451(January):569–72.

26. Cho JY, Sternberg PW (2014) Multilevel modulation of a sensory motor circuit during C. elegans sleep and arousal. *Cell* 156(1–2):249–260.

27. Hendricks JC, et al. (2000) Rest in Drosophila is a sleep-like state. *Neuron*. doi:10.1016/S0896-6273(00)80877-6.

28. Nath RD, et al. (2017) The Jellyfish Cassiopea Exhibits a Sleep-like State. *Curr Biol*. doi:10.1016/j.cub.2017.08.014.

29. Steriade M, McCormick DA, Sejnowski TJ (1993) Thalamocortical oscillations in the sleeping and aroused brain. *Science (80-)*. doi:10.1126/science.8235588.

30. Nitz DA, Van Swinderen B, Tononi G, Greenspan RJ (2002) Electrophysiological correlates of rest and activity in Drosophila melanogaster. *Curr Biol*. doi:10.1016/S0960-9822(02)01300-3.

31. Bushey D, Tononi G, Cirelli C (2015) Sleep- and wake-dependent changes in neuronal activity and reactivity demonstrated in fly neurons using in vivo calcium imaging. *Proc Natl Acad Sci*. doi:10.1073/pnas.1419603112.

32. Kato S, et al. (2015) Global Brain Dynamics Embed the Motor Command Sequence of Caenorhabditis elegans. *Cell* 163(3):656–669.

33. Nichols ALA, Eichler T, Latham R, Zimmer M (2017) A global brain state underlies C.

elegans sleep behavior. *Science (80-)* 356(1247):eaam6851:1-9.

34. Van Buskirk C, Sternberg PW (2007) Epidermal growth factor signaling induces behavioral quiescence in Caenorhabditis elegans. *Nat Neurosci* 10(10):1300–1307.

35. Van Buskirk C, Sternberg PW (2010) Paired and LIM class homeodomain proteins coordinate differentiation of the C. elegans ALA neuron. *Development*. doi:10.1242/dev.040881.

36. Monsalve GC, Van Buskirk C, Frand AR (2011) LIN-42/PERIOD controls cyclical and developmental progression of C. elegans molts. *Curr Biol*. doi:10.1016/j.cub.2011.10.054.

37. Singh K, et al. (2011) C. elegans notch signaling regulates adult chemosensory response and larval molting quiescence. *Curr Biol*. doi:10.1016/j.cub.2011.04.010.

38. Turek M, Lewandrowski I, Bringmann H (2013) An AP2 transcription factor is required for a sleep-active neuron to induce sleep-like quiescence in C. elegans. *Curr Biol* 23(22):2215–2223.

39. Turek M, Besseling J, Spies JP, König S, Bringmann H (2016) Sleep-active neuron specification and sleep induction require FLP-11 neuropeptides to systemically induce sleep. *Elife*. doi:10.7554/eLife.12499.

40. Hill AJ, Mansfield R, Lopez JMNG, Raizen DM, Buskirk C Van (2014) Cellular Stress Induces a Protective Sleep-like State in C. elegans. *Curr Biol*:1–7.

41. Choi S, Chatzigeorgiou M, Taylor KP, Schafer WR, Kaplan JM (2013) Analysis of NPR-1 reveals a circuit mechanism for behavioral quiescence in C.elegans. *Neuron* 78(5):869–880.

42. Nelson MD, et al. (2013) The neuropeptide NLP-22 regulates a sleep-like state in Caenorhabditis elegans. *Nat Commun*. doi:10.1038/ncomms3846.

43. Wu Y, Masurat F, Preis J, Bringmann H (2018) Sleep Counteracts Aging Phenotypes to Survive Starvation-Induced Developmental Arrest in C. elegans. *Curr Biol* 28:1–14.

44. Nath RD, Chow ES, Wang H, Schwarz EM, Sternberg PW (2016) C. elegans Stress-Induced Sleep Emerges from the Collective Action of Multiple Neuropeptides. *Curr Biol*. doi:10.1016/j.cub.2016.07.048.

45. Nelson MD, et al. (2014) FMRFamide-like FLP-13 Neuropeptides Promote Quiescence following Heat Stress in Caenorhabditis elegans. *Curr Biol*. doi:10.1016/j.cub.2014.08.037.

46. Trojanowski NF, Raizen DM (2016) Call it Worm Sleep. *Trends Neurosci* 39(2):54–62.

47. Zimmerman JE, Naidoo N, Raizen DM, Pack AI (2008) Conservation of sleep: insights from non-mammalian model systems. *Trends Neurosci*. doi:10.1016/j.tins.2008.05.001.

48. Kayser MS, Biron D (2016) Sleep and development in genetically tractable model organisms. *Genetics*. doi:10.1534/genetics.116.189589.

49. Ghosh R, Emmons SW (2008) Episodic swimming behavior in the nematode C. elegans. *J Exp Biol* 211(Pt 23):3703–3711.

50. Gonzales DL, et al. (2017) Scalable electrophysiology in intact small animals with nanoscale suspended electrode arrays. *Nat Nanotechnol* 12:694–691.

51. Ghosh R, Emmons SW (2010) Calcineurin and Protein kinase G regulate C. Elegans behavioral quiescence during locomotion in liquid. *BMC Genet*. doi:10.1186/1471-2156-

11-7.

52. McCloskey RJ, Fouad AD, Churgin MA, Fang-Yen C (2017) Food Responsiveness Regulates Episodic Behavioral States in *Caenorhabditis elegans*. *J Neurophysiol*:jn.00555.2016.

53. Churgin MA, McCloskey RJ, Peters E, Fang-Yen C (2017) Antagonistic serotonergic and octopaminergic neural circuits mediate food-dependent locomotory behavior in Caenorhabditis elegans. *J Neurosci* 39(33):7811–7823.

54. Iannacone MJ, et al. (2017) The RFamide receptor DMSR-1 regulates stress-induced sleep in C. elegans. *Elife*. doi:10.7554/eLife.19837.

55. DeBardeleben HK, Lopes LE, Nessel MP, Raizen DM (2017) Stress-induced sleep after exposure to ultraviolet light is promoted by p53 in caenorhabditis elegans. *Genetics*. doi:10.1534/genetics.117.300070.

56. Churgin MA, et al. (2017) Longitudinal imaging of caenorhabditis elegans in a microfabricated device reveals variation in behavioral decline during aging. *Elife*. doi:10.7554/eLife.26652.

57. Iwanir S, et al. (2013) The microarchitecture of C. elegans behavior during lethargus: homeostatic bout dynamics, a typical body posture, and regulation by a central neuron. *Sleep*. doi:10.5665/sleep.2456.

58. Driver RJ, Lamb AL, Wyner AJ, Raizen DM (2013) DAF-16/FOXO regulates homeostasis of essential sleep-like behavior during larval transitions in C. elegans. *Curr Biol*. doi:10.1016/j.cub.2013.02.009.

59. Tramm N, Oppenheimer N, Nagy S, Efrati E, Biron D (2014) Why do sleeping nematodes

adopt a hockey-stick-like posture? *PLoS One*. doi:10.1371/journal.pone.0101162.

60. Schwarz J, Spies J-P, Bringmann H (2012) Reduced muscle contraction and a relaxed posture during sleep-like Lethargus. *Worm* 1(1):12–4.

61. Schwarz J, Lewandrowski I, Bringmann H (2011) Reduced activity of a sensory neuron during a sleep-like state in Caenorhabditis elegans. *Curr Biol* 21(24):R983–R984.

62. Nagy S, et al. (2014) Homeostasis in C. elegans sleep is characterized by two behaviorally and genetically distinct mechanisms. *Elife*. doi:10.7554/eLife.04380.

63. McClanahan PD, Xu JH, Fang-Yen C (2017) Comparing: Caenorhabditis elegans gentle and harsh touch response behavior using a multiplexed hydraulic microfluidic device. *Integr Biol (United Kingdom)*. doi:10.1039/c7ib00120g.

64. Trojanowski NF, Nelson MD, Flavell SW, Fang-Yen C, Raizen DM (2015) Distinct Mechanisms Underlie Quiescence during Two Caenorhabditis elegans Sleep-Like States. *J Neurosci* 35(43):14571–14584.

65. Skora S, Mende F, Zimmer M (2018) Energy Scarcity Promotes a Brain-wide Sleep State Modulated by Insulin Signaling in C. elegans. *Cell Rep* 22(4):953–966.

66. Nguyen JP, et al. (2015) Whole-brain calcium imaging with cellular resolution in freely behaving Caenorhabditis elegans. *Proc Natl Acad Sci U S A*:33.

67. Venkatachalam V, et al. (2015) Pan-neuronal imaging in roaming Caenorhabditis elegans. *Proc Natl Acad Sci U S A*:201507109.

68. Nguyen JP, Linder AN, Plummer GS, Shaevitz JW, Leifer AM (2017) Automatically tracking neurons in a moving and deforming brain. *PLoS Comput Biol* 13(5):e1005517.

69. Schrödel T, Prevedel R, Aumayr K, Zimmer M, Vaziri A (2013) Brain-wide 3D imaging of neuronal activity in Caenorhabditis elegans with sculpted light. *Nat Methods* 10(10):1013–20.

70. Prevedel R, et al. (2014) Simultaneous whole-animal 3D imaging of neuronal activity using light-field microscopy. *Nat Methods* 11(7):727–30.

71. You Y jai, Kim J, Raizen DM, Avery L (2008) Insulin, cGMP, and TGF-β Signals Regulate Food Intake and Quiescence in C. elegans: A Model for Satiety. *Cell Metab*. doi:10.1016/j.cmet.2008.01.005.

72. Prahlad V, Cornelius T, Morimoto RI (2008) Regulation of the cellular heat shock response in Caenorhabditis elegans by thermosensory neurons. *Science (80-)*. doi:10.1126/science.1156093.

73. Clark DA, Biron D, Sengupta P, Samuel ADT (2006) The AFD sensory neurons encode multiple functions underlying thermotactic behavior in Caenorhabditis elegans. *J Neurosci* 26(28):7444–7451.

74. Ramot D, MacInnis BL, Goodman MB (2008) Bidirectional temperature-sensing by a single thermosensory neuron in C. elegans. *Nat Neurosci* 11(8):908–915.

75. Han B, et al. (2017) Dopamine signaling tunes spatial pattern selectivity in C. elegans. *Elife* 6:1–14.

76. Li W, Kang L, Piggott BJ, Feng Z, Xu XZS (2011) The neural circuits and sensory channels mediating harsh touch sensation in Caenorhabditis elegans. *Nat Commun*. doi:10.1038/ncomms1308.

77. Hsu A-L, Murphy CT, Kenyon C (2003) Regulation of aging and age-related disease by

DAF-16 and heat-shock factor. *Science* 300(5622):1142–1145.

78. Ogg S, et al. (1997) The Fork head transcription factor DAF-16 transduces insulin-like metabolic and longevity signals in C. elegans. *Nature* 389(6654):994–999.

79. Henderson ST, Johnson TE (2001) daf-16 integrates developmental and environmental inputs to mediate aging in the nematode Caenorhabditis elegans. *Curr Biol*. doi:10.1016/S0960-9822(01)00594-2.

80. Kopito RB, Levine E (2014) Durable spatiotemporal surveillance of Caenorhabditis elegans response to environmental cues. *Lab Chip*. doi:10.1039/c3lc51061a.

81. Van Voorhies WA, Ward S (1999) Genetic and environmental conditions that increase longevity in Caenorhabditis elegans decrease metabolic rate. *Proc Natl Acad Sci*. doi:10.1073/pnas.96.20.11399.

82. San-Miguel A, Lu H (2013) Microfluidics as a tool for C . elegans research. *Wormbook*, pp 1–19. The C. ele.

83. Nagy S, Raizen DM, Biron D (2014) Measurements of behavioral quiescence in Caenorhabditis elegans. *Methods* 68(3):500–507.

Author contributions:

D.L.G. conceived, performed and analyzed experiments. J.Z. performed and analyzed whole-brain imaging experiments. J.T.R. directed the research. D.L.G. and J.T.R. co-wrote the paper. All authors read and commented on the manuscript.

Competing financial interests:

The authors declare no competing financial interests.